π^+ absorption on N and Ar

D. Rowntree,[5] D. Androić,[9] G. Backenstoss,[1] D. Bosnar,[9] H. Breuer,[4] T. Dooling,[7] M. Furić,[9] P. A. M. Gram,[3] N. K. Gregory,[5] A. Hoffart,[2,8] C. H. Q. Ingram,[8] A. Klein,[7] K. Koch,[8] J. Köhler,[1] B. Kotliński,[8] M. Kroedel,[1] G. Kyle,[6] A. Lehmann,[1,8] A. O. Mateos,[5] K. Michaelian,[8] T. Petković,[9] M. Planinić,[9] R. P. Redwine,[5] N. Šimičević,[5] R. Trezeciak,[2] H. J. Weyer,[1,8] M. Wildi,[1] and K. E. Wilson[5]

(LADS Collaboration)

[1]*University of Basel, CH-4056 Basel, Switzerland*
[2]*University of Karlsruhe, D-76128 Karlsruhe, Germany*
[3]*LAMPF, Los Alamos, Los Alamos, New Mexico 87545*
[4]*University of Maryland, College Park, Maryland 20742*
[5]*Massachusetts Institute of Technology, Cambridge, Massachusetts 02139*
[6]*New Mexico State University, Las Cruces, New Mexico 88003*
[7]*Old Dominion University, Norfolk, Virginia 23529*
[8]*Paul Scherrer Institute, CH-5232 Villigen PSI, Switzerland*
[9]*University of Zagreb, HR-10000 Zagreb, Croatia*

(Received 14 May 1999; published 4 October 1999)

The absorption of positive pions on N and Ar has been studied for $T_{\pi^+}=118$, 162, and 239 MeV. A precise determination has been made of the total absorption cross section for each energy and target nucleus. Comparisons are made with prior LADS results on ^{2}H, ^{3}He, and ^{4}He. In addition, results are presented for the detected multiplicities of emitted protons, neutrons, and deuterons following pion absorption.
[S0556-2813(99)06610-8]

PACS number(s): 25.80.Ls, 25.10.+s, 25.60.Dz

I. INTRODUCTION

Pion-nucleus interactions have long been used to investigate the nuclear force in the nuclear medium. Currently, the most interesting aspect of the nuclear force accessible through pion absorption is the possibility of a multinucleon (>2) component of the strong force. There is an expanding body of evidence from pion absorption experiments which indicates that a significant fraction of the absorption process directly involves at least three nucleons [1,2]. If a distinct multinucleon absorption mechanism does exist, it will demonstrate a facet of the strong nuclear force that has not yet appeared in any other subfield of nuclear physics. Difficulties persist in demonstrating its presence, however, since it may not be clearly distinguished from an initial state interaction (ISI) or a final state interaction (FSI) [3–5]. In fact, basic properties of the absorption process, such as the total cross section and the number of participating nucleons, are still not well known for nuclei heavier than ^{4}He.

Several early experiments gave indications that the absorption process could be significantly modified by the presence of more than two nucleons. The results of a measurement of the total absorption cross section on a series of nuclei ranging from ^{7}Li to ^{209}Bi at six energies in the Δ-resonance energy region were published by Ashery *et al.* [6]. The general result of this experiment was that the total absorption cross section increases with A in proportion to the cross sectional area of the nucleus. For very light nuclei initial experiments indicated an even larger A dependence, with a large increase in the total absorption cross section between ^{3}He [7,8] and ^{4}He [9]. However, in a recent paper [10] we have shown that this increase is more moderate than previously indicated; a fact that had already been suggested by the results on ^{4}He of Steinacher *et al.* [11].

For $A>4$, the particle multiplicities following absorption are not well known. Absorption on a two nucleon pair is well documented, and kinematic signatures of this process are visible in absorption on heavy nuclei. It was expected that the average nucleon multiplicity would be larger than two due mainly to ISI and FSI. Results from the (π^+,p) experiment of McKeown *et al.* [12,13] indicated that the average number of nucleons involved ranged from about three on ^{12}C to more than five on ^{181}Ta. These were significantly higher than expected, suggesting that rescattering processes and perhaps a multinucleon absorption process play a very significant role.

We present the results of an experiment using the Large Acceptance Detector System (LADS) to study the absorption of positive pions on N and Ar at 118, 162, and 239 MeV incident kinetic energies. Quantitative results are given for an analysis using techniques suitable for heavy nuclei and comparisons are made to prior results on ^{2}H, ^{3}He, and ^{4}He which used the available kinematical constraints more fully [3,10,14–16]. In particular, the total absorption cross section and particle multiplicities are presented (see [4,5] for some differential investigations).

II. EXPERIMENTAL APPARATUS

The LADS detector (see Fig. 1) was constructed at the Paul Scherrer Institute in Villigen, Switzerland to study multinucleon final states resulting from pion absorption. To be appropriate for this task, the detector needed to be able to simultaneously detect, identify, and measure the momenta of multiple final state particles. This required a detector of close

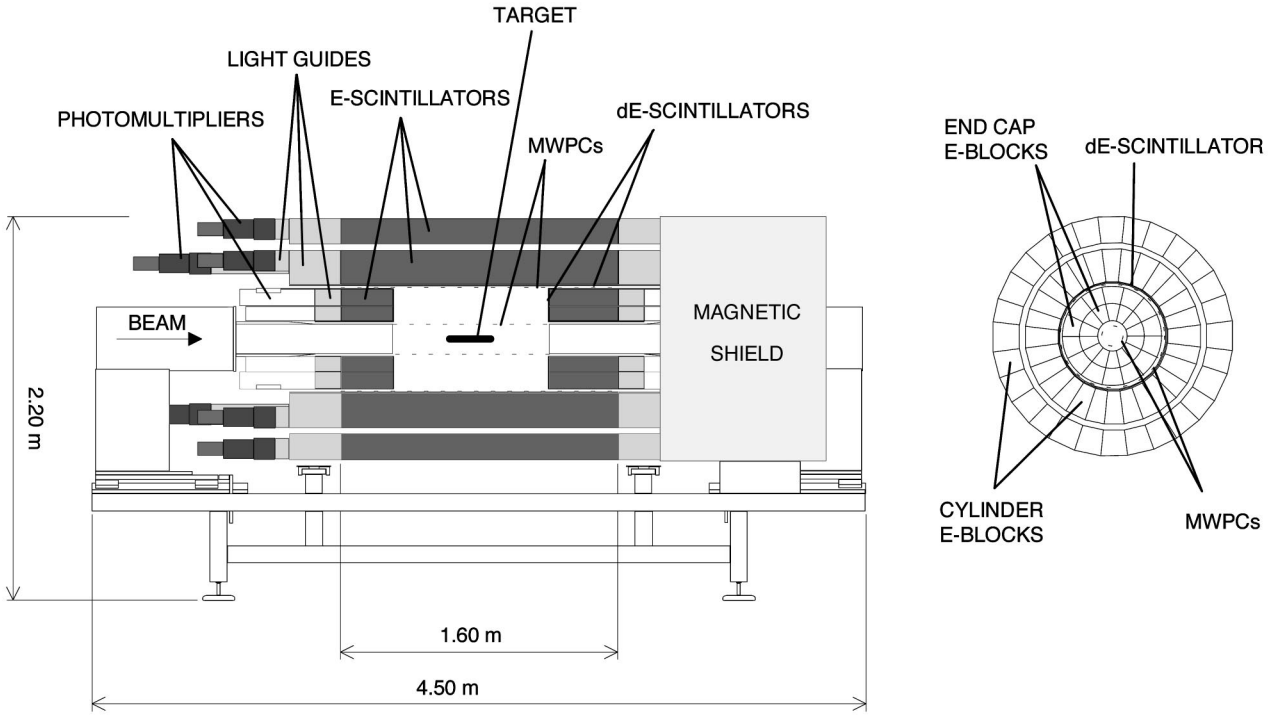

FIG. 1. The LADS detector from Ref. [17].

to 4π sr solid angle coverage with low energy thresholds and good energy and trajectory resolution.

The LADS detector achieved these goals by using a thick cylinder of plastic scintillator, endcaps of the same material, and two coaxial cylindrical multiwire proportional chambers (MWPCs). The cylinder scintillators were arranged in 28 trapezoidally-shaped sectors each consisting of a 160 cm long dE-E-E scintillator telescope. Each scintillator bar was read out by photomultiplier tubes on each end, giving energy and rough position information. The inner radius of the cylinder was 30 cm, and the thickness was 35.5 cm, sufficient to stop a 200 MeV normally incident proton.

The scintillator endcaps were inserted into the open ends of the cylinder. Each consisted of two rings of scintillator, divided azimuthally into 14 sectors. The beam pipe passed through an 8 cm radius hole through the center of each—the only region uncovered by plastic scintillator. The front face of each scintillator endcap was covered by a thin dE scintillator, also in 14 sectors.

The entire inner face of the cylinder (including the region between the cylinder and the endcaps) was covered by the outer MWPC. The inner MWPC lay in the 90 cm gap between the endcaps.

At the center of LADS, there was a cylindrical, high pressure ($\leqslant$100 bar) thin-walled gas target made from carbon fiber. It was 25.7 cm in length and 2 cm in radius. The energy threshold of the detector was dominated by energy loss in the walls of the target and in the MWPCs. It depended on the trajectory of the particle, ranging for protons from about 16 to about 22 MeV.

The experiment was performed in the πM1 area at the Paul Scherrer Institute. A narrow beam was selected with a combination of scintillator elements, the last of which was a 1 cm radius, 0.1 cm thick counter mounted on the end of a long light guide in front of the target. This counter selected about 10^5 pions/s from an incident flux of typically 3×10^6/s. Additional details about the detector, data acquisition, and analysis systems may be found in Ref. [17].

III. DATA ANALYSIS

There were several steps which led to the determination of particle multiplicities following absorption. First, pion absorption events were isolated and then classified according to the number and type of emitted particle (e.g., $2p1n$). These yields were converted to cross sections by normalizing to the number of beam particles and target scatterers. Finally, corrections were made for various inefficiencies of the detector. A more complete description of the analysis can be found in Ref. [18].

A. Particle reconstruction

A particle was identified as charged or neutral depending on whether the appropriate dE counter fired. The MWPCs were used to identify the few ($\approx$1%) charged particles that slipped through the cracks between the dEs. The finite beam size, multiple scattering, or nuclear reactions could cause a particle to deposit energy into adjacent sectors. The likelihood of this occurring was significant, about 30% for an energetic charged proton. This was much more likely than the possibility that an accompanying neutral particle was in a sector adjacent to a charged particle. Therefore, sectors

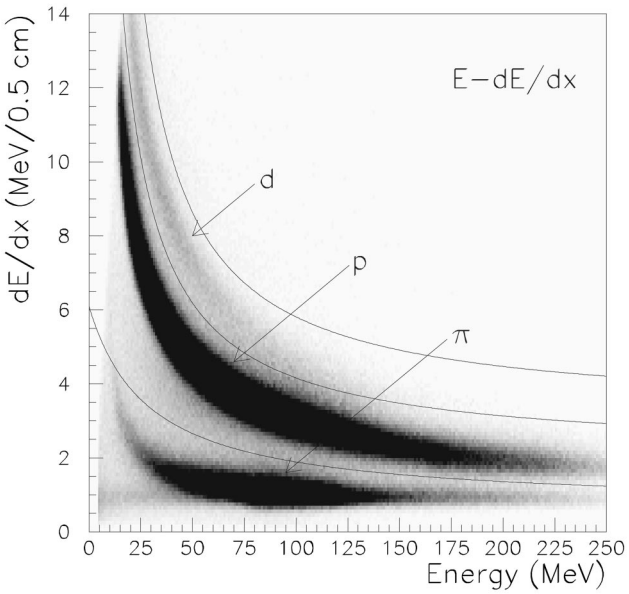

FIG. 2. An E-dE/dx plot for particles in the cylinder scintillators. The data are from 239 MeV π^+ incident on N. The curves show the tests used for PID.

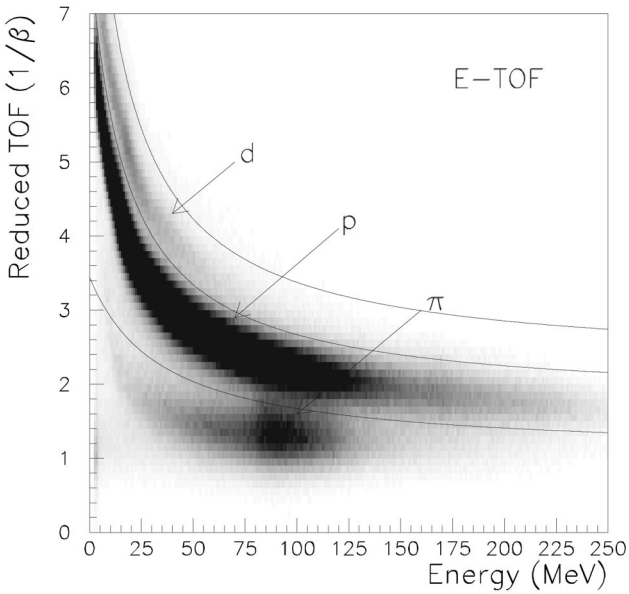

FIG. 3. An E-TOF plot for particles in the cylinder scintillators. The data are from 239 MeV π^+ incident on N. The curves show the tests used for PID.

which recorded a neutral particle adjacent to a charged particle were reconstructed into a single charged particle.

Several additional constraints were applied to those particles which were detected. First, particles which had less than 2.5 MeV of associated light detected were interpreted as noise and were ignored in the analysis. For charged particles this restriction increased the effective detector threshold by 2.5 MeV. This restriction was also applied to neutral particles. Second, any particle that had a large reduced time-of-flight (TOF) ($1/\beta$, or the amount of time in ns needed for the particle to traverse 30 cm) was ignored in the analysis. This cut eliminated many random hits, but only very low energy particles in real coincidence with the pion absorption event.

B. Charged particle identification

Particle identification (PID) was performed using a combination of E-dE/dx and E-TOF techniques. If more than 10 MeV of light was detected in the E blocks, then the primary method was E-dE/dx. Figure 2 shows a typical spectrum for this method, with the cuts used to identify pions, protons, and deuterons shown as hyperbolic lines. When less than 10 MeV was detected in the E blocks, the method used was E-TOF, illustrated in Fig. 3. Bands associated with the different particle types are clearly separated. For the majority of the particles detected, the PID method applied was E-dE/dx. E-TOF was generally used only for the least energetic particles, although some use was also made of the TOF information to resolve ambiguities in the identification of higher energy particles. The above techniques were sufficient to correctly identify over 90% of the charged particles detected. Corrections to account for the remainder are described later (Secs. III D and III G).

C. Neutral particle identification

Both neutrons and photons were common among the final state particles detected by LADS. High energy neutrons were assumed to come from the reactions being studied, while low energy neutrons were associated with evaporation from the final state nucleus. High energy photons were assumed to come from π^0 decay following single charge exchange (SCX) reactions, and the low energy photons were associated with electromagnetic deexcitation of residual nuclei. Different treatments were required for the different cases. The low energy particles were ignored, the high energy neutrons were included in the multiplicities, and the high energy photons indicated that an absorption event did not occur.

The quantities used to identify each case were the particle's reduced TOF and the light deposited in the scintillators. The reduced TOF, illustrated in Fig. 4, was initially used to separate neutrons from photons. Because it was more important in the analysis to ensure that neutrons were counted than γ's excluded, the cut appearing in Fig. 4 is offset from the center of the valley. To separate energetic from evaporation neutrons, a cut was applied to the reduced TOF corresponding to 20 ± 10 MeV. The separation of π^0 decay photons from nuclear deexcitation photons is discussed in Sec. III F.

D. Reaction corrections

In the analysis of pion absorption experiments of the type described here, a significant problem is the possibility of mistakenly labeling a proton as a pion or mistakenly labeling a pion as a proton. This section will investigate the magnitude of the probability of the former, and Sec. III G will examine the magnitude of the latter.

The situation in which a proton is mistakenly identified as a pion is frequently due to reactions. The term ''reaction''

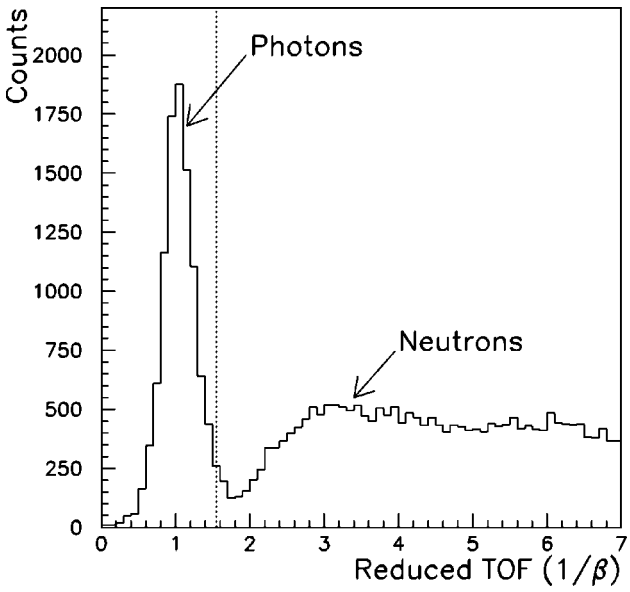

FIG. 4. The reduced TOF spectrum for neutrals detected after the interaction of 162 MeV π^+'s with Ar. The cut used to separate γ's from neutrons is shown as a dotted line.

used in this context usually refers to a particle undergoing a nuclear interaction in the scintillator such that not all of the kinetic energy of the particle is seen as light. We will define a reaction as having occurred any time a charged particle is labeled by PID as something which it is not. Various resolution effects are thus included with the nuclear processes.

In order to determine the probability of mistakenly identifying a proton as a pion, data were used from the interaction of 239 MeV π^+'s with ^{3}He. A data sample was filtered out in which each event had exactly three charged particles detected. The three particles were numbered randomly, and the first two were required to be identified as a proton in the cylinder by the PID procedure, and to have been recorded in both MWPCs. These two tracks were used to make a clean cut on the target region in both r and z. A missing mass was calculated from these two protons, and a cut applied at the proton mass, ensuring that PID was correct for these two particles, an absorption reaction occurred, and that their energy information was correct.

Now the energy of the third proton was calculated from the initial state and the energies of the first two protons. The third proton was subjected to all of the PID tests discussed previously. The probability for a proton to be mistakenly identified as a pion was then determined as a function of proton energy. It rose smoothly from 0% at low energy to above 11% above 200 MeV.

Similar methods to the above were used to determine the fraction of the time that a deuteron was mistaken as a proton [using the ^{4}He(π^+,ppd) reaction] and that a proton was mistaken for a deuteron [using the ^{3}He(π^+,ppp) reaction].

E. Event normalization

To obtain a cross section from the number of events of a particular type (e.g. $2p1n$), the following expression was used:

$$\sigma_{2p1n}=\frac{1}{N_\pi\times N_{\text{nuclei}}}\sum_{\text{trigger types}}\left[N_{2p1n}^{\text{trigger type}}\times\frac{N_{\text{scalers}}^{\text{trigger type}}}{N_{\text{events on tape}}^{\text{trigger type}}}\right],$$

where N_π is the corrected number of pions on target and N_{nuclei} is the number of target scatterers. The sum is over the separately prescaled experimental trigger types [17]. For each, it corrects the yield from the analysis ($N_{2p1n}^{\text{trigger type}}$) by the ratio of the number of events counted in the scalers ($N_{\text{scalers}}^{\text{trigger type}}$) to the number of events recorded on tape ($N_{\text{events on tape}}^{\text{trigger type}}$), accounting simultaneously for the computer dead time and the prescale factors.

A beam pion is defined by a coincidence between several counters. Both timing and pulse height values for these counters are required to be within tight limits to reduce contamination from extraneous particles and pion reactions in the beam counters. Additional corrections were made to the beam flux for the effect of π^+ decay.

It was also necessary to correct the counted beam flux to account for any pions which missed the target. Attenuation of the beam due to pion interactions was calculated from the known cross sections to be $2\%\pm1\%$. To estimate the fraction of the beam missing the target due to multiple scattering and beam divergence, events from interactions in the air before and after the target were used. Events were selected which had a two track vertex from the MWPCs. The ratio of the number of events within the target's radius to the total number of events was measured for 1 cm slices before and after the target, which were then averaged. The percentage of the pions missing the target varied from 4% to 9%.

The number of target scatterers was straightforwardly calculated from the temperature and pressure of the target gas, both of which were monitored during the experiment. For the pressures involved in this experiment, deviations from the ideal gas law become important. The factor of compressibility, which is unity for an ideal gas, amounted to as much as a 5% correction [19].

F. Single charge exchange subtraction

If a photon converts in the scintillator, a substantial fraction of its energy will typically be detected. Thus the light deposited can be used as a good estimate of the photon's energy. Nuclear deexcitation photons are usually under 10 MeV while SCX photons are typically high energy. This wide separation makes the identification by the amount of deposited light feasible. Figure 5 shows a spectrum of deposited light for detected photons. Those photons depositing greater than 14 MeV energy were identified as resulting from SCX, and those depositing less were ignored.

The LADS photon detection efficiency was approximately 30%. Since a π^0 decays into two photons, roughly half of the SCX events had one or two detected photons. The remaining SCX events were handled by subtracting a scaled fraction of events with detected γ's. The first step in this process is to determine the γ detection efficiency for the LADS detector. This was done under the assumption that the probability of detecting each of the two photons was independent. This assumption is not strictly correct, since the directions and energies of the photons are kinematically linked. However,

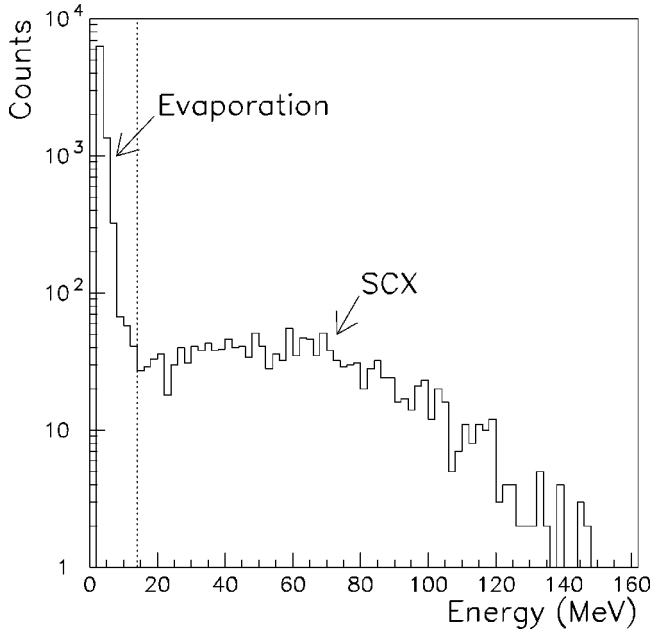

FIG. 5. The spectrum of energy calibrated pulse heights for photons after the interaction of 162 MeV π^+'s with Ar. The cut used to separate low energy γ's from SCX γ's is shown as a dotted line.

since LADS covers such a large fraction of 4π steradians, there should be little error introduced by this assumption.

Cross sections were separately calculated for the cases in which one photon was detected and the cases in which two photons were detected. A comparison of these cases gave the γ detection efficiency ϵ_γ. Then the final cross section (e.g., for σ_{1p1n}) was determined from

$$\sigma_{1p1n}=\sigma_{1p1n}^{0\gamma}-f_{\mathrm{SCX}}\times\sigma_{1p1n}^{\geqslant 1\gamma},$$

where

$$f_{\mathrm{SCX}}=\frac{(1-\epsilon_\gamma)^2}{2\epsilon_\gamma(1-\epsilon_\gamma)+\epsilon_\gamma^2}.$$

The uncertainty associated with this correction was substantial, in particular for the cross section with only one detected charged particle, where the SCX cross section is significant in comparison to the absorption cross section. To significantly reduce the uncertainties, the limitation was applied that if only one charged particle was detected, it had to have over 35 MeV of associated light. Even with these limitations, the total SCX yield was as high as 28% of the total absorption yield for N at 239 MeV, and the associated uncertainty in the correction dominated the error for that measurement.

G. Pion contamination

Although the various PID methods correctly identified most of the final state charged pions, some still slipped through the cuts. There is a large scattering cross section for small angles, so the first step was to limit the acceptance of the detector by demanding the detection of at least one charged particle with a polar angle greater than 15°. The method used to correct for the remaining contamination was similar to that used for calculating reaction corrections. A sample of events which included a charged pion in the final state was selected from data with a ^{2}H target by using only MWPC information. These events were then passed through the analysis chain to determine their effect on the cross section. Roughly 1% of the scattered pions were misidentified as protons, leading to small corrections to the total cross section and corrections of varying magnitude to the individual multiplicities. These corrections were performed by subtracting a fraction of the cross section for detected pions.

TABLE I. Total cross sections for π^+ absorption (in mb) for three different incident pion kinetic energies. In this table, the results for ^{2}H and ^{3}He are from [14], and the results for ^{4}He are from [10].

Target	118 MeV	162 MeV	239 MeV
^{2}H	11.5±0.4	10.9±0.3	4.3±0.2
^{3}He	27.3±0.8	24.7±0.7	10.0±0.4
^{4}He	52±4	51±5	27±2
N	182±10	163±11	107±10
Ar	393±21	366±22	282±21

H. Events without an MWPC vertex

Events in which no vertex was calculated by the MWPCs, either because no charged particle passed through both chambers or because of inefficiency of the MWPCs, were also analyzed to produce cross sections for the different particle multiplicities. The analysis was performed essentially independently, with different reaction correction, pion contamination, and neutron detection efficiency numbers being

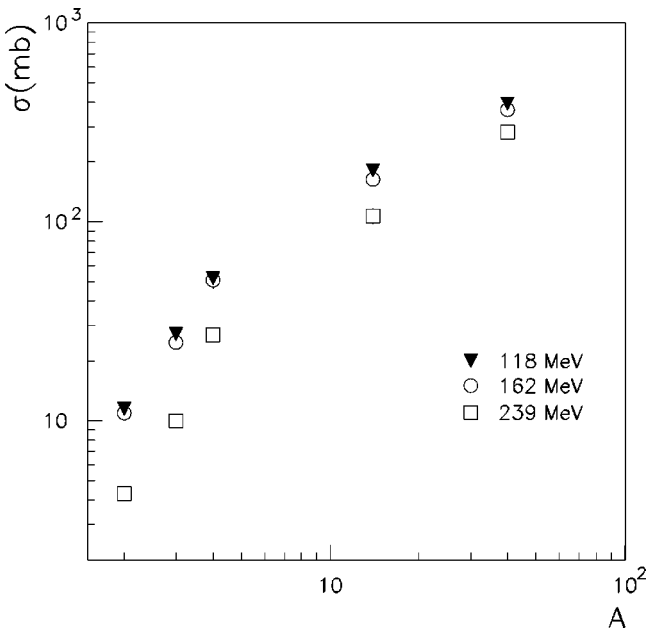

FIG. 6. The total absorption cross sections are shown as a function of A. The triangles are for an incident pion energy of 118 MeV; the circles, 162 MeV; and the squares, 239 MeV. Uncertainties are almost always smaller than the size of the symbol.

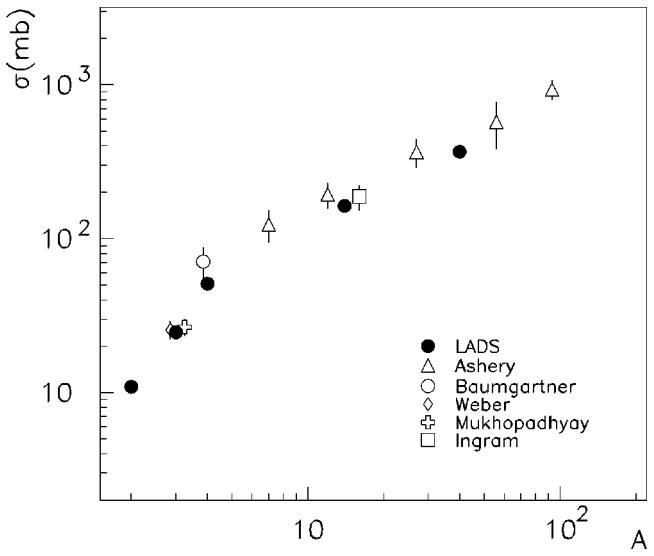

FIG. 7. A comparison between the total absorption cross sections from this detector and those from previous experiments in the vicinity of 165 MeV. The solid circles show the LADS results; the diamond is from Weber *et al.* [7]; the cross is from Mukhopadhyay *et al.* [8]; the open circle is from Baumgartner *et al.* [9]; the triangles are from Ashery *et al.* [6]; and the square is from Ingram *et al.* [21].

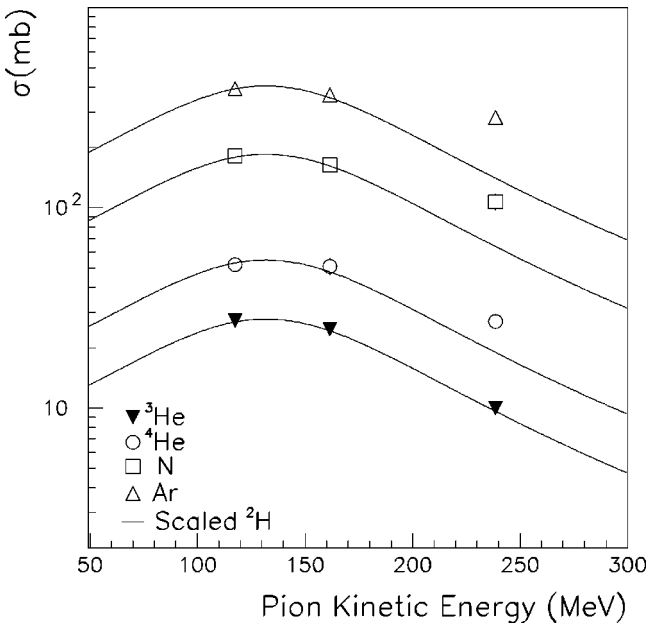

FIG. 8. The total absorption cross sections are shown as a function of the incident π^+ energy. The solid triangles are for ^{3}He; the circles for ^{4}He; the squares for N; and the open triangles for Ar. The curves are proportional to a parametrization of the ^{2}H cross section [22].

calculated. The resulting cross sections were added to those with MWPC information to produce the final results.

I. Background subtraction

The above analysis was repeated for empty target runs, and the results subtracted from the final cross sections. The background subtraction was a significant correction only for the events without an MWPC track. For these events, the uncertainties are significantly larger because of the smaller signal-to-noise ratio (the worst case for the N and Ar total cross sections was 1–to–1 for Ar at 118 MeV). However, the increased uncertainties only affect a small portion of the cross section ($<10\%$ of the total for Ar at 118 MeV).

J. Neutron detection efficiency

The neutron detection efficiency was determined by using the reaction $^4\mathrm{He}(\pi^+,pppn)$. By considering cases where all three protons were detected, the missing mass reconstructed to that of a neutron, and the missing momentum had a greater than 30° opening angle with each of the protons, it was possible to select a clean sample of neutrons with which to measure the detection efficiency. The results were averaged over the neutron energy and angle, and the determined neutron detection efficiency was $\epsilon_n = 36 \pm 4\%$.

In the process of determining the neutron multiplicities, small corrections were made for contamination from photons, contamination from the products of scattering and reactions in the scintillator, and small amounts of background noise in the detector. After the detected neutron multiplicities were determined, the neutron detection efficiency was used to correct the results. No significant cross sections were found with greater than three neutrons, so this was taken as the maximum. The strength with three detected neutrons was divided by ϵ_n^3, and then the strength with fewer neutrons was corrected accordingly. The process was then repeated for two and one detected neutrons.

IV. RESULTS AND DISCUSSION

A. Total absorption cross sections

The total cross sections for pion absorption are presented in Table I. The reported uncertainties include both the systematic and statistical errors. The normalization uncertainty is the most important for the total cross sections, dominated by the uncertainty in the fraction of the pions which pass through the target.

Since the geometrical and kinematic acceptance of the detector is nearly complete, the correspondence between the observed and the actual total absorption cross sections is close, and no acceptance corrections were applied. Consideration of the particle distributions, and of the acceptance corrections applied to the He data [3,10,14–16], indicated that such corrections would be small compared to the quoted uncertainties.

The total absorption cross sections reported in Table I are graphed as a function of A in Fig. 6. The cross sections at 118 and 162 MeV are approximately equal, with the cross section at 239 MeV being significantly smaller.

Of previous experiments that measured total absorption cross sections, the most extensive was that of Ashery *et al.* [6]. In that experiment, measurements were made of the total reaction cross section and the pion scattering cross section. The absorption cross section was calculated by taking the difference, and then subtracting an estimate of the SCX cross

TABLE II. Detected final state energetic particle multiplicities following π^+ absorption on N (in mb). The cross section is first given for a particular number of charged particles (protons and deuterons together) accompanied by any number of neutrons. These values are then broken down according to the number of neutrons and the proton and deuteron mix. The efficiencies of the detector have been corrected, but limitations in its acceptance have not. For cross sections consistent with zero, the reported value is the 95% confidence upper limit.

$T_\pi = 118$ MeV						
Charge multiplicity	(mb)	Deuterons	$0n$	$1n$	$2n$	$\geqslant 3n$
$1C$	40.9 ± 2.8	0	14.6 ± 3.0	21.8 ± 2.2	4.0 ± 0.9	0.2 ± 0.1
		1	0.7 ± 0.3	<0.3	0.1 ± 0.1	–
$2C$	114.9 ± 6.2	0	71.3 ± 5.2	28.3 ± 2.9	3.3 ± 0.6	0.4 ± 0.2
		1	8.1 ± 1.6	3.3 ± 0.7	0.3 ± 0.1	–
$3C$	24.4 ± 1.7	0	12.1 ± 1.2	4.5 ± 0.6	0.4 ± 0.1	–
		1	6.0 ± 0.8	1.4 ± 0.3	–	–
$\geqslant 4C$	1.4 ± 0.1	0	0.5 ± 0.1	0.2 ± 0.1	–	–
		1	0.6 ± 0.1	0.1 ± 0.1	–	–
$T_\pi = 162$ MeV						
Charge multiplicity	(mb)	Deuterons	$0n$	$1n$	$2n$	$\geqslant 3n$
$1C$	27.2 ± 4.4	0	8.6 ± 4.2	14.4 ± 1.6	2.8 ± 0.4	0.9 ± 0.3
		1	0.8 ± 0.3	<0.2	<0.1	0.1 ± 0.1
$2C$	98.7 ± 5.4	0	56.1 ± 4.7	28.3 ± 2.7	4.7 ± 1.0	0.4 ± 0.2
		1	5.4 ± 1.2	3.2 ± 0.7	0.5 ± 0.2	–
$3C$	33.8 ± 2.4	0	15.6 ± 1.6	7.4 ± 0.9	1.0 ± 0.2	0.1 ± 0.1
		1	7.1 ± 0.9	2.5 ± 0.4	0.2 ± 0.1	–
$\geqslant 4C$	3.6 ± 0.3	0	1.1 ± 0.2	0.5 ± 0.1	0.1 ± 0.1	–
		1	1.5 ± 0.2	0.5 ± 0.1	–	–
$T_\pi = 239$ MeV						
Charge multiplicity	(mb)	Deuterons	$0n$	$1n$	$2n$	$\geqslant 3n$
$1C$	11.2 ± 5.1	0	<8.1	7.7 ± 1.4	2.5 ± 0.6	0.6 ± 0.3
		1	<0.6	<0.4	0.1 ± 0.1	–
$2C$	57.0 ± 3.9	0	26.7 ± 3.5	19.3 ± 1.5	5.2 ± 1.0	0.8 ± 0.3
		1	2.1 ± 0.7	2.3 ± 0.5	0.5 ± 0.2	0.1 ± 0.1
$3C$	31.9 ± 2.3	0	12.4 ± 1.4	8.8 ± 0.9	2.0 ± 0.4	0.2 ± 0.1
		1	4.9 ± 0.7	2.9 ± 0.4	0.7 ± 0.2	–
$\geqslant 4C$	6.3 ± 0.6	0	1.8 ± 0.3	1.2 ± 0.2	0.3 ± 0.1	–
		1	2.2 ± 0.3	1.3 ± 0.2	0.1 ± 0.1	–

section. Figure 7 shows a comparison between the current 162 MeV results and the 165 MeV results of Ref. [6]. While consistent within uncertainties, the results of Ref. [6] appear systematically higher than the current data. Part of this difference is due to the subtraction of too small a value for the SCX cross section [20]. The ^{16}O result of Ingram *et al.* [21] is in better agreement with the current results.

Also shown in Fig. 7 are measurements on ^{3}He by Weber *et al.* [7] and Mukhopadhyay *et al.* [8], and on ^{4}He by Baumgartner *et al.* [9]. As mentioned in the Introduction, these results had suggested an anomalously large rise in the cross section between these two nuclei, creating much interest in the search for new absorption mechanisms. The LADS data modify the previous view significantly, although the rise from ^{2}H to ^{4}He remains large.

Figure 8 shows the total absorption cross section again, but as a function of the incident pion energy. The curves on this figure represent the absorption cross section on deuterium scaled by factors of 2.3, 4.5, 15, and 33 in order to fit them to the 118 and 162 MeV data. For ^{3}He the cross section at 239 MeV has fallen similarly to that for the deuteron, while for the heavier nuclei, even ^{4}He, the decline is smaller. This behavior is broadly consistent with the underlying absorption cross section being dominated by the same mechanism as absorption on the deuteron: at high incident energies a pion which loses energy by a quasielastic scattering in the nucleus remains at an energy where the absorption probability is large. Thus the slower decline in the total cross section for heavier nuclei could be a reflection of such cascadelike processes preceding a Δ-dominated two-nucleon absorption.

B. Detected multiplicities

Observed final state multiplicities after absorption on N and Ar are given in Tables II and III. These results are cor-

TABLE III. Detected final state energetic particle multiplicities following π^+ absorption on Ar (in mb). The organization is the same as in Table II.

$T_\pi = 118$ MeV						
Charge multiplicity	(mb)	Deuterons	$0n$	$1n$	$2n$	$\geqslant 3n$
$1C$	134.8±7.6	0	39.6±8.8	71.7±5.7	18.9±3.4	3.2±1.1
		1	<1.3	1.3±1.3	<0.7	0.1±0.1
$2C$	222.0±12.0	0	110.1±10.0	68.5±6.2	13.3±2.4	2.0±0.7
		1	15.6±2.9	10.7±1.9	1.9±0.5	0.3±0.1
$3C$	34.5±2.4	0	16.3±1.6	7.4±0.8	1.4±0.3	–
		1	6.9±0.9	2.3±0.4	0.2±0.1	–
$\geqslant 4C$	1.5±0.2	0	0.6±0.1	0.1±0.1	0.1±0.1	–
		1	0.4±0.1	0.1±0.1	–	–
$T_\pi = 162$ MeV						
Charge multiplicity	(mb)	Deuterons	$0n$	$1n$	$2n$	$\geqslant 3n$
$1C$	96.2±9.6	0	19.0±9.3	45.2±3.0	27.5±5.3	3.3±1.1
		1	0.7±0.5	<1.6	<0.8	0.3±0.2
$2C$	211.7±11.5	0	88.1±9.5	70.2±5.0	22.5±3.8	4.4±1.5
		1	11.2±2.4	11.6±1.9	3.2±0.8	0.5±0.2
$3C$	54.1±3.8	0	21.8±2.3	13.3±1.3	3.3±0.7	0.4±0.2
		1	9.3±1.3	5.0±0.7	1.1±0.3	–
$\geqslant 4C$	4.0±0.4	0	1.3±0.2	1.0±0.2	–	–
		1	1.3±0.2	0.4±0.1	0.1±0.1	–
$T_\pi = 239$ MeV						
Charge multiplicity	(mb)	Deuterons	$0n$	$1n$	$2n$	$\geqslant 3n$
$1C$	50.7±10.3	0	<16.0	25.0±2.5	15.9±1.7	7.7±2.7
		1	<0.3	1.7±0.6	1.1±0.4	0.2±0.2
$2C$	152.2±9.0	0	44.7±7.6	54.5±3.5	25.0±3.4	7.9±2.7
		1	5.3±1.6	9.3±1.4	4.2±0.8	1.4±0.5
3C	67.9±4.8	0	20.2±2.9	20.7±1.9	6.1±1.0	1.7±0.6
		1	8.3±1.4	7.9±1.0	2.7±0.6	0.4±0.2
$\geqslant 4C$	10.3±0.9	0	2.8±0.5	2.7±0.4	0.4±0.1	0.1±0.1
		1	2.8±0.4	1.7±0.2	0.5±0.2	–

rected for reaction losses and detector efficiencies as discussed above. The reported uncertainties include both the systematic and statistical errors, with the former generally dominating; here the uncertainties due to pion contamination, the SCX cross section, and the neutron detection efficiency are the main contributors.

The main goal of the analysis reported here was the determination of reliable total absorption cross sections, for which correction of the yields for the detector's geometrical acceptance and energy threshold was not necessary—these limitations of the detector had significant effects only on the observed multiplicities, not on the total yield. Since these limitations most commonly cause a final state particle to be lost they generally cause high final state multiplicities to be understated and lower multiplicities to be overstated in Tables II and III. Rudimentary estimates indicate that in severe cases (e.g. a three nucleon final state at 118 MeV) roughly 70% of the actual strength is observed.

The relative strength of the $1C$ (one charged particle) channel rises with A and decreases with incident energy, with a low of 3% on ^{4}He at 239 MeV [10] and a high of 34% on Ar at 118 MeV. The energy dependence may be largely due to the detection threshold, while the A dependence is probably related to the increased availability of neutrons which carry away part of the energy. In fact, a general trend which is evident is that the number of neutrons participating in the reaction is increasing with A faster than the number of protons. The ratio of pn to pp multiplicities increases from an average of under 10% on ^{4}He [10] to about 30% on N, and to about 55% on Ar. For ppn and ppp, the average ratio goes from 1.9 [10] to 1.9 to 3.4 for the three nuclei.

Significant cross sections for four or more energetic nucleons in the final state were found, especially at 239 MeV. The fraction of the total cross section with more than three nucleons (a deuteron counts as two nucleons) was about 15% for ^{4}He [10], 35% for N, and 40% for Ar at this

energy. Since correcting for acceptance would increase these cross sections, high multiplicity final states constitute an important part of the absorption process for N and Ar.

The experiments closest to LADS in solid angle coverage are those using the BGO ball at LAMPF. This large solid angle detector has been used to study π^+ reactions for a large range of incident pion energies and target masses [23–25]. The data most easily compared to the present results are from the 150 MeV measurement on ^{12}C [23]. In order to compare the BGO ball results to the current N results, they need to be scaled up by $(14/12)^{2/3}$ to account for the different number of nucleons, and down by 0.9 (the ratio between absorption on ^{2}H at 162 and 150 MeV), which leaves them approximately unchanged. Their $2p$ cross section of 110 ± 22 mb can include additional protons, deuterons, or single neutrons, but events with two or more detected neutrons are vetoed. Constructing the approximately equivalent result from Table II gives 121 mb, in good agreement. A more significant difference is found in the $3p$ cross section. Their result of 14 mb should be compared to 25 mb, which is almost a factor of 2 different. However, a reanalysis of the BGO ball data, extrapolating the cross section using a lower threshold for protons, yielded a corrected $3p$ inclusive cross section of 21 ± 5 mb [26], in better agreement. The application of acceptance corrections to our data would cause this difference to increase. Should this difference become significant, the discrepancy is possibly attributable to the difficulty associated with correcting the BGO ball's results for its higher energy threshold ($\approx$25 MeV) and smaller solid angular coverage ($\approx$84% of 4π sr). Finally, it should be mentioned that their cross section for detecting an energetic deuteron is also lower by about a factor of 2; no acceptance corrections were made to this result, so the higher threshold and smaller acceptance may account for the difference.

Figure 9 shows the average number of energetic final state nucleons for each combination of target and incident pion energy. The values for ^{3}He and ^{4}He are calculated from the results reported in Refs. [10,14]. For N and Ar, rudimentary corrections for the detector acceptance and energy threshold were made by using a phase space distribution of nucleons to approximate the final state. This method, while acceptable because of the almost complete coverage of the detector, is quite rough. An uncertainty of half the size of the correction was included in the error bars.

For ^{3}He, one can see that the average number is approximately independent of energy. The average number of nucleons participating in the absorption process increases with A from 2.3 for ^{3}He to 2.7 for Ar at 118 MeV, from 2.3 to 3.1 at 162 MeV, and from 2.4 to 3.7 at 239 MeV. The fact that this average has a significant increase with A at 239 MeV, while remaining almost constant at 118 MeV, is consistent with the dominance of the Δ resonance. For the lower incident pion energies, any ISI would move the pion far off the resonance peak, and thus the larger A does not have a large effect on the average number of nucleons.

Previously, the best knowledge of the number of nucleons participating in the absorption reaction for $A>4$ came from the results of the McKeown *et al.* [12] experiment. In this

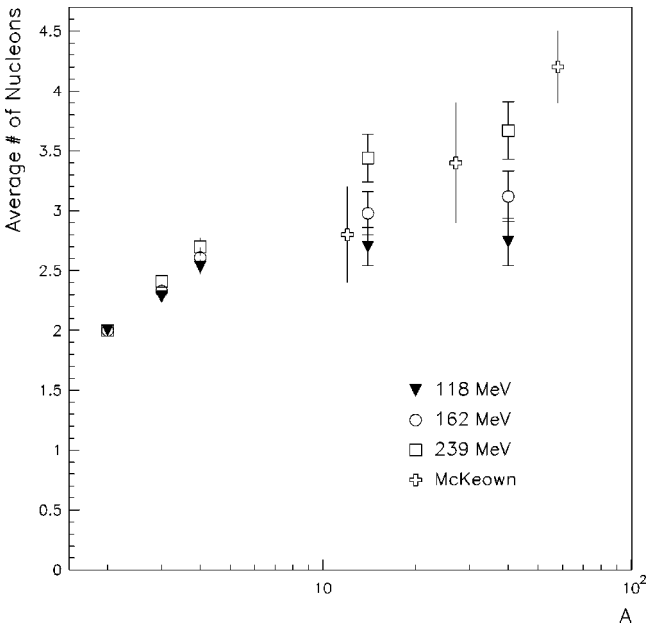

FIG. 9. The average number of final state energetic nucleons, with corrections for detector inefficiencies and a very rudimentary correction for thresholds and acceptances, is shown as a function of A.

experiment, singles proton energy spectra were measured, and a rapidity analysis was used to extract the average number of participating nucleons. The reported results, shown in Fig. 9 for comparison, were averages over incident π^+ energies of 100, 160, and 220 MeV. The results of Ref. [12] are in good agreement with the current ones for low A, but rise at a more rapid rate, and the trend possibly disagrees for high A. It may be noted that the current experiment is a more direct measurement of the nucleon multiplicity than that of Ref. [12], and thus less subject to assumptions and possible biases.

V. SUMMARY

The absorption of π^+ in the $\Delta(1232)$-resonance energy region has been examined for N and Ar, and compared to prior results on ^{2}H, ^{3}He, and ^{4}He. Total absorption cross sections are reported, along with the breakup into channels with different numbers of energetic final state nucleons. The N and Ar cross sections are the most precise measurements on nuclei with $A>4$ so far.

ACKNOWLEDGMENTS

We thank the technical staff of the Paul Scherrer Institute for the support provided to this experiment. This work was supported in part by the German Bundesministerium für Forschung und Technologie (BMFT), the German Internationales Büro der Kernforschungsanlage Jülich, the Swiss National Science Foundation, the U.S. Department of Energy (DoE), and the National Science Foundation (NSF).

[1] H. J. Weyer, Phys. Rep. **195**, 295 (1990).

[2] D. Ashery and J. P. Schiffer, Annu. Rev. Nucl. Part. Sci. **36**, 207 (1986).

[3] G. Backenstoss, D. Bosnar, H. Breuer, H. Döbbeling, T. Dooling, M. Furić, P. A. M. Gram, N. K. Gregory, A. Hoffart, C. H. Q. Ingram, A. Klein, K. Koch, J. Köhler, B. Kotliński, M. Kroedel, G. Kyle, A. Lehmann, A. O. Mateos, K. Michaelian, T. Petković, R. P. Redwine, D. Rowntree, U. Sennhauser, N. Šimičević, R. Trezeciak, H. Ullrich, M. Wang, M. H. Wang, H. J. Weyer, M. Wildi, and K. E. Wilson, Phys. Lett. B **379**, 60 (1996).

[4] D. Androić, G. Backenstoss, D. Bosnar, H. Breuer, H. Döbbeling, T. Dooling, M. Furić, P. A. M. Gram, N. K. Gregory, A. Hoffart, C. H. Q. Ingram, A. Klein, K. Koch, J. Köhler, B. Kotliński, M. Kroedel, G. Kyle, A. Lehmann, A. O. Mateos, K. Michaelian, T. Petković, R. P. Redwine, D. Rowntree, U. Sennhauser, N. Šimičević, R. Trezeciak, H. Ullrich, M. Wang, M. H. Wang, H. J. Weyer, M. Wildi, and K. E. Wilson, Phys. Rev. C **53**, 2591 (1996).

[5] B. Kotliński, D. Androić, G. Backenstoss, D. Bosnar, H. Breuer, H. Döbbeling, T. Dooling, M. Furić, P. A. M. Gram, N. K. Gregory, A. Hoffart, C. H. Q. Ingram, A. Klein, K. Koch, J. Köhler, M. Kroedel, G. Kyle, A. Lehmann, A. O. Mateos, K. Michaelian, T. Petković, M. Planinić, R. P. Redwine, D. Rowntree, U. Sennhauser, N. Šimičević, R. Trezeciak, H. Ullrich, H. J. Weyer, M. Wildi, and K. E. Wilson, Eur. Phys. J. A **1**, 435 (1998).

[6] D. Ashery, I. Navon, G. Azuelos, H. K. Walter, H. J. Pfeiffer, and F. W. Schlepütz, Phys. Rev. C **23**, 2173 (1981).

[7] P. Weber, G. Backenstoss, M. Iżycki, P. Slavisberg, R. J. Powers, M. Steinacher, S. Cierjacks, A. Hoffart, B. Rzehorz, H. Ullrich, H. J. Weyer, N. Bosnar, M. Furić, T. Petković, and N. Šimičević, Nucl. Phys. **A534**, 541 (1991).

[8] S. Mukhopadhyay, S. Levenson, R. E. Segel, G. Garino, D. F. Geesaman, J. P. Schiffer, G. Stephans, B. Zeidman, E. Ungricht, H. Jackson, R. Kowalczyk, D. Ashery, E. Piasetsky, M. Moinester, I. Navon, L. C. Smith, R. C. Minehart, G. S. Das, R. R. Whitney, R. McKeown, B. Anderson, R. Madey, and J. Watson, Phys. Rev. C **43**, 957 (1991).

[9] M. Baumgartner, H. P. Gubler, G. R. Plattner, W. D. Ramsay, H. W. Roser, I. Sick, and P. Zupranski, Nucl. Phys. **A399**, 451 (1983).

[10] A. O. Mateos, D. Androić, G. Backenstoss, D. Bosnar, H. Breuer, H. Döbbeling, T. Dooling, M. Furić, P. A. M. Gram, N. K. Gregory, A. Hoffart, C. H. Q. Ingram, A. Klein, K. Koch, J. Köhler, B. Kotliński, M. Kroedel, G. Kyle, A. Lehmann, K. Michaelian, T. Petković, M. Planinić, R. P. Redwine, D. Rowntree, U. Sennhauser, N. Šimičević, R. Trezeciak, H. Ullrich, M. Wang, M. H. Wang, H. J. Weyer, M. Wildi, and K. E. Wilson, Phys. Rev. C **58**, 942 (1998).

[11] M. Steinacher, G. Backenstoss, M. Iżycki, P. Salvisberg, P. Weber, H. J. Weyer, A. Hoffart, B. Rzehorz, H. Ullrich, M. Dzemidzić, M. Furić, and T. Petković, Nucl. Phys. **A517**, 413 (1990).

[12] R. D. McKeown, S. J. Sanders, J. P. Schiffer, H. E. Jackson, M. Paul, J. R. Specht, E. J. Stephenson, R. P. Redwine, and R. E. Segel, Phys. Rev. Lett. **44**, 1033 (1980).

[13] R. D. McKeown, S. J. Sanders, J. P. Schiffer, H. E. Jackson, M. Paul, J. R. Specht, E. J. Stephenson, R. P. Redwine, and R. E. Segel, Phys. Rev. C **24**, 211 (1981).

[14] T. Alteholz, D. Androić, G. Backenstoss, D. Bosnar, H. Breuer, A. Brković, H. Döbbeling, T. Dooling, W. Fong, M. Furić, P. A. M. Gram, N. K. Gregory, J. P. Haas, A. Hoffart, C. H. Q. Ingram, A. Klein, K. Koch, J. Köhler, B. Kotliński, M. Kroedel, G. Kyle, A. Lehmann, Z. N. Lin, G. Mahl, A. O. Mateos, K. Michaelian, S. Mukhopadhyay, T. Petković, R. P. Redwine, D. Rowntree, R. Schumacher, U. Sennhauser, N. Šimičević, F. D. Smit, G. van der Steenhoven, D. R. Tieger, R. Trezeciak, H. Ullrich, M. Wang, M. H. Wang, H. J. Weyer, M. Wildi, and K. E. Wilson, Phys. Rev. Lett. **73**, 1336 (1994).

[15] A. Lehmann, D. Androić, G. Backenstoss, D. Bosnar, H. Breuer, H. Döbbeling, T. Dooling, M. Furić, P. A. M. Gram, N. K. Gregory, A. Hoffart, C. H. Q. Ingram, A. Klein, K. Koch, J. Köhler, B. Kotliński, M. Kroedel, G. Kyle, A. O. Mateos, K. Michaelian, T. Petković, M. Planinić, R. P. Redwine, D. Rowntree, U. Sennhauser, N. Šimičević, R. Trezeciak, H. Ullrich, M. Wang, M. H. Wang, H. J. Weyer, M. Wildi, and K. E. Wilson, Phys. Rev. C **55**, 2931 (1997).

[16] A. Lehmann, D. Androić, G. Backenstoss, D. Bosnar, H. Breuer, H. Döbbeling, T. Dooling, M. Furić, P. A. M. Gram, N. K. Gregory, A. Hoffart, C. H. Q. Ingram, A. Klein, K. Koch, J. Köhler, B. Kotliński, M. Kroedel, G. Kyle, A. O. Mateos, K. Michaelian, T. Petković, M. Planinić, R. P. Redwine, D. Rowntree, U. Sennhauser, N. Šimičević, R. Trezeciak, H. Ullrich, M. Wang, M. H. Wang, H. J. Weyer, M. Wildi, and K. E. Wilson, Phys. Rev. C **56**, 1872 (1997).

[17] T. Alteholz, D. Androić, G. Backenstoss, D. Bosnar, H. Breuer, A. Brković, H. Döbbeling, T. Dooling, W. Fong, M. Furić, P. A. M. Gram, N. K. Gregory, J. P. Haas, A. Hoffart, C. H. Q. Ingram, A. Klein, K. Koch, J. Köhler, B. Kotliński, M. Kroedel, G. Kyle, A. Lehmann, Z. N. Lin, G. Mahl, A. O. Mateos, K. Michaelian, S. Mukhopadhyay, T. Petković, M. Planinić, R. P. Redwine, D. Rowntree, R. Schumacher, U. Sennhauser, N. Šimičević, F. D. Smit, G. van der Steenhoven, D. R. Tieger, R. Trezeciak, H. Ullrich, M. Wang, M. H. Wang, H. J. Weyer, M. Wildi, and K. E. Wilson, Nucl. Instrum. Methods Phys. Res. A **373**, 374 (1996).

[18] D. Rowntree, Ph.D. thesis, Massachusetts Institute of Technology, 1995.

[19] L'Air Liquide (Firm), *Encyclopedie des Gaz* (Elsevier, New York, 1976).

[20] D. Ashery, D. F. Geesaman, R. J. Holt, H. E. Jackson, J. R. Specht, K. E. Stephenson, R. E. Segel, P. Zupranski, H. W. Baer, J. D. Bowman, M. D. Cooper, M. Leitch, A. Erell, J. J. Comuzzi, R. P. Redwine, and D. R. Tieger, Phys. Rev. C **30**, 946 (1984).

[21] C. H. Q. Ingram, P. A. M. Gram, J. Jansen, R. E. Mischke, J. Zichy J. Bolger, E. T. Boschitz, G. Pröbstle, and J. Arvieux, Phys. Rev. C **27**, 1578 (1983).

[22] B. Ritchie, Phys. Rev. C **44**, 533 (1991).

[23] R. D. Ransome, C. L. Morris, V. R. Cupps, R. W. Fergerson, J. A. McGill, D. L. Watson, J. D. Zumbro, B. G. Ritchie, J. R. Comfort, J. R. Tinsley, R. A. Loveman, S. Dawson, A. Green, P. C. Gugelot, and C. Fred Moore, Phys. Rev. C **45**, R509 (1992).

[24] R. D. Ransome, C. L. Morris, M. K. Jones, B. G. Ritchie, D. L. Watson, J. A. McGill, K. Pujara, D. B. Clayton, I. Brown, P. Campbell, and C. Fred Moore, Phys. Rev. C **46**, 273 (1992).

[25] M. Jones, R. D. Ransome, V. R. Cupps, R. W. Fergerson, C. L. Morris, J. A. McGill, J. D. Zumbro, J. R. Comfort, B. G. Ritchie, J. R. Tinsley, P. C. Gugelot, and C. Fred Moore, Phys. Rev. C **48**, 2800 (1993).

[26] R. A. Giannelli, B. G. Ritchie, J. M. Applegate, E. Beck, J. Beck, A. O. Vanderpoel, C. L. Morris, M. Rahwool-Sullivan, M. K. Jones, R. D. Ransome, M. Yadav, D. L. Watson, K. O. Oganesjan, E. A. Pasyuk, F. F. Guber, and A. I. Reshetin (unpublished); R. D. Ransome (private communication).